



Influence of the activation atmosphere on the hydrodesulfurization of Co-Mo/SBA-15 catalysts prepared from sulfur-containing precursors

G. Alonso-Núñez^{a,*}, J. Bocarando^a, R. Huirache-Acuña^b, L. Álvarez-Contreras^c, Z.-D. Huang^d, W. Bensch^d, G. Berhault^e, J. Cruz^f, T.A. Zepeda^a, S. Fuentes^a

^a Universidad Nacional Autónoma de México, Centro de Nanociencias y Nanotecnología, Ensenada, Baja California, C.P. 22860, Mexico

^b Universidad Michoacana de San Nicolás de Hidalgo, Morelia, Michoacán, Mexico

^c Centro de Investigación en Materiales Avanzados S. C., Chihuahua, Chih., C.P. 31109, Mexico

^d Institut für Anorganische Chemie, Christian-Albrechts University of Kiel, Max-Eyth-Str. 2, D-24118 Kiel, Germany

^e Institut de Recherches sur la Catalyse et l'Environnement de Lyon, CNRS Université Lyon 1, 02 Av. A. Einstein, 69100 Villeurbanne, France

^f Facultad de Ciencias Químicas e Ingeniería, Universidad Autónoma de Baja California, Tijuana, B. C., Mexico

ARTICLE INFO

Article history:

Received 4 November 2011

Received in revised form 13 January 2012

Accepted 15 January 2012

Available online 25 January 2012

Keywords:

Hydrodesulfurization

SBA-15

Activation

ATM

Dithiocarbamate

Confinement effect

ABSTRACT

Mesoporous SBA-15 material was used as support of binary Co-Mo hydrodesulfurization (HDS) catalysts prepared using a novel approach based on the use of already sulfided precursors (ammonium tetrathiomolybdate and cobalt diethyldithiocarbamate). The effects of atmosphere and activation temperature were studied to optimize the preparation of highly active CoMo/SBA-15 hydrodesulfurization catalysts. Two sets of catalysts were synthesized using either a N₂/H₂ (10% H₂) or a H₂/H₂S (15% H₂S) atmosphere at three different temperatures of activation (723, 773 and 823 K). The catalysts were tested in the HDS of dibenzothiophene (DBT) and the catalysts were characterized by N₂ physisorption, X-ray diffraction (XRD), scanning electron microscopy (SEM) and high-resolution transmission electron microscopy (HRTEM). The use of already sulfided precursors leads to a homogeneous dispersion of the active phase inside the SBA-15 channels. Moreover, the N₂/H₂ activation procedure at 723 K allows obtaining optimized HDS active catalysts. Finally, a confinement effect of MoS₂ slabs inside the SBA-15 channels leads to a high selectivity along the direct desulfurization pathway.

© 2012 Elsevier B.V. All rights reserved.

1. Introduction

Nowadays, the processing of “more dirty” feeds containing larger amounts of sulfur has become more and more urgently needed and a new generation of transition metal sulfide-based catalysts with higher activities, greater selectivity, and better resistance to poisoning is required. Using high-performance hydrodesulfurization (HDS) catalysts is then necessary to achieve lower sulfur concentration levels satisfying environmental restrictions [1].

Typically, hydrotreatment (HDT) reactions are catalyzed by sulfided Co(Ni)Mo(W) catalysts supported on alumina [2]. The origin of the almost exclusive use of alumina as support has been ascribed to its outstanding textural and mechanical properties and its relatively low cost [3]. However, the presence of undesirable strong metal-support interaction when using alumina has triggered research devoted to the development of new supports for HDT applications [4–13]. Thus, more recently, research concerning

the development of highly dispersed active phase on zeolites or mesoporous materials has been very intense in order to respect the stringent regulations concerning the maximum amount of sulfur admitted in fuels. Some results have been presented before in publications concerning the effect of support in hydrotreating catalysts for ultra clean fuels [12,14].

On the other hand, the catalyst activation is also a crucial step for the physicochemical properties (nature, composition and dispersion of the active phase) and consequently for activity and selectivity properties. In this respect, the temperature of treatment used during this step can affect the degree of reduction and sulfidation as well as the dispersion of the active phase. The influence of activation over the HDS of dibenzothiophene (DBT) on CoMo/Al₂O₃, NiMo/Al₂O₃, Ru/MgF₂ materials has been investigated extensively [15–23].

The influence of atmosphere during the decomposition of ammonium tetrathiomolybdate for the activation of unpromoted and cobalt-promoted alumina-supported MoS₂ catalysts was also investigated by Pawelec et al. [24]. This study showed a strong influence of the activation procedure. For the unpromoted catalyst, the most efficient treatment was related to the use of a 10% H₂S/H₂ atmosphere while the cobalt-promoted catalyst needed

* Corresponding author. Tel.: +52 646 174 46 02.

E-mail address: galonso@cny.unam.mx (G. Alonso-Núñez).

a more complex activation combining first a calcination treatment followed by successive H_2S/H_2 and H_2 treatments. However, in the case of CoMo/SBA-15 catalytic systems, the influence of atmosphere and temperature used during the activation of this type of catalysts has not been reported in the literature. Moreover, the control of the dispersion of the active phase inside the SBA-15 channels remains challenging [25]. The classical wetness impregnation based on the use of ammonium heptamolybdate and cobalt nitrate was not found to be successful in order to locate MoS_2 slabs inside the SBA-15 mesopores [26,27]. An alternative solution was then envisaged by Vradman et al. [28] leading to a good dispersion of WS_2 slabs but using a complicated procedure based on the sonication of a $W(CO)_6$ -sulfur-diphenylmethane solution with SBA-15. Another interesting approach is based on the use of already-sulfided precursors. This kind of precursors is well-known and was envisaged extensively in previous studies [29–36]. Recent results have also shown that the use of an already-sulfided precursor, ammonium tetrathiomolybdate (ATM), was an interesting simple solution to achieve a better dispersion of MoS_2 slabs inside the SBA-15 channels [10] even if progress is still needed in this respect. Indeed, in this study, ATM was stirred in aqueous solution with $CoS_x/SBA-15$ solids obtained by impregnation of cobalt acetate on the SBA-15 support followed by sulfidation. This approach led to a limited intimate mixing between cobalt and molybdenum and therefore to a non-ideal homogeneous dispersion inside the mesopores. One possible solution is the use of both already sulfided precursors of cobalt and molybdenum through a successive mixing of the SBA-15 support with two different solutions of ATM and cobalt diethyldithiocarbamate.

The objective of the present study will then be to determine the optimized conditions for the activation of CoMo/SBA-15 catalysts prepared through a novel approach based on the use of already-sulfided Co and Mo precursors. After contacting SBA-15 with cobalt diethyldithiocarbamate and ATM, two sets of catalysts were then activated varying atmosphere and temperature. These catalysts were characterized by N_2 -physisorption, X-ray Diffraction (XRD), scanning electron microscopy with field emission (FESEM) and high-resolution transmission electron microscopy (HRTEM). The sulfide catalysts were tested in the hydrodesulfurization of DBT. This reaction was selected for catalyst screening purposes because (1) DBT is a typical sulfur-containing hydrocarbon present in the petroleum fraction of high-boiling oil or coal derived liquids [2] and (2) because of the absence of any diffusion limitation for DBT molecule to entry into the porous structure of the SBA-15-supported catalysts [28].

2. Experimental

2.1. Support and catalyst preparation

The SBA-15 support material was prepared following the synthesis route reported in reference [18]. The metal based composition for each catalyst was set to 12 wt% of Mo and 3 wt% of Co. 2 g of SBA-15 powder (sieved between 80 and 120 μm) was first stirred for 4 h in 100 mL of a saturated chloroform solution of cobalt diethyldithiocarbamate, $CoS_2CN(C_2H_5)_2$ (CoDETC). The solvent was then removed by filtration and the obtained product was dried under vacuum overnight.

The dried product was then stirred in 150 mL of a saturated aqueous solution of ammonium tetrathiomolybdate at 298 K. After 4 h of stirring, the product was filtered without washing and then activated. The precursor ATM was synthesized according to the synthesis method reported in [10] and the CoDETC was obtained from Aldrich.

Table 1

List of catalysts synthesized with different activation atmospheres.

	Atmosphere	Temperature (K)		
		723	773	823
Set 1	N_2/H_2 ($H_2 = 10\%$)	S1A	S1B	S1C
Set 2	H_2S/H_2 ($H_2S = 10\%$)	S2A	S2B	S2C

2.2. Activation of Co-Mo/SBA-15

Activation was performed by heating ex situ the as-obtained solids under a N_2/H_2 (10% (v/v) H_2) mixture (set 1) or under a H_2S/H_2 (15% (v/v) H_2S) mixture (set 2) from 298 K to $T^{\circ} sulf$ ($T^{\circ} sulf = 723, 773$ or 823 K) at a heating rate of 4K/min. Once the desired value of $T^{\circ} sulf$ was reached, the temperature was held constant for 4 h under the flow of the activating gas mixture. After this period, the gas was switched from the H_2S/H_2 (15% (v/v) H_2S) or N_2/H_2 (10% (v/v) H_2) mixture to pure N_2 flow while the temperature was decreased to 298 K. The as-obtained catalysts were then kept under nitrogen atmosphere to prevent oxidation before being transferred to the batch reactor for HDS reaction. The catalysts are labeled according to Table 1.

2.3. Sample characterization

Nitrogen adsorption–desorption measurements were carried out at 77 K on a Quantachrom Autosorb. Samples were degassed under flowing argon at 573 K for 4 h before nitrogen adsorption. The surface area measurements were performed according to the Brunauer–Emmett–Teller (BET) method. XRD patterns were collected on a Philips X Pert MPD diffractometer at room temperature using monochromatized Cu $K\alpha$ radiation ($\lambda = 1.54056 \text{ \AA}$) in a $10\text{--}70^\circ$ 2θ range. FESEM was used to observe any morphological variation in catalysts due to the applied gas flow used during the activation procedure. Scanning electron micrographs were obtained with a JSM-7401F microscope (cold FE, 30 kV). The transmission electron microscopy (TEM) used was a JEOL JEM 2200FS microscope (200 kV). The samples for FESEM and TEM analysis were prepared by dispersing the powder products as a slurry in acetone before drying it on a Cu grid.

2.4. Catalytic activity and selectivity

HDS of DBT was carried out in a Parr model 4520 high-pressure batch reactor. 1.0 g of the catalyst and 150 mL of the freshly prepared solution of DBT in decalin (5%, w/w) were introduced into the reactor. The reactor was then purged and pressurized to 3.4 MPa (490 psi) with hydrogen and then heated up to 623 K with continuous stirring at 600 rpm. The reaction was followed during 5 h by analyzing samples every 30 min using a PerkinElmer XL gas chromatograph equipped with an OV-17 packed column.

The main reaction products for the HDS of DBT are biphenyl (BP) formed by direct C–S bond cleavage of DBT (the so-called direct desulfurization pathway, DDS) and cyclohexylbenzene (CHB) formed by an initial hydrogenation of one of the aromatic rings of tetrahydrodibenzothiophene (THDBT) followed by C–S bond rupture (the hydrogenating pathway, HYD). The HYD/DDS selectivity ratio is based on the product concentration ratio according to Eq. (1).

$$HYD/DDS = (THDBT + CHB)/BP \quad (1)$$

The rate constant was determined from the DBT conversion as function of time assuming DBT conversion as a pseudo zero-order reaction [37].

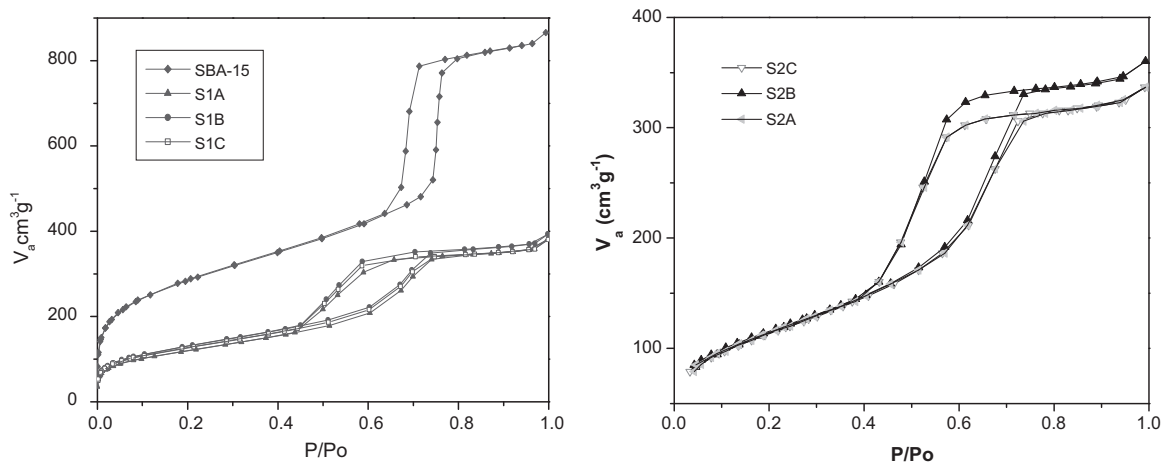


Fig. 1. Nitrogen adsorption–desorption isotherms of the SBA-15 support and of N_2/H_2 activated CoMo/SBA-15 catalysts (set 1) (a) and of H_2/H_2S activated CoMo/SBA-15 catalysts (set 2) (b).

3. Results and discussion

3.1. Structural characterization of the CoMo/SBA-15 catalysts

3.1.1. Textural properties

Nitrogen adsorption–desorption isotherms of the SBA-15 support and of the two sets of catalysts activated under N_2/H_2 (set 1) or H_2/H_2S (set 2) are shown in Fig. 1. All samples exhibit the typical type-IV isotherms for mesoporous materials with cylindrical pores. The SBA-15 support shows a typical type H1 adsorption–desorption hysteresis loop characteristic for cylindrical pore channels. The loop seems particularly developed in this case indicating the presence of a large amount of mesopores [38].

The N_2 adsorption–desorption isotherms of the CoMo/SBA-15 catalysts are substantially different from the ones observed for the SBA-15 support alone even if type IV isotherms are still obtained showing that the mesoporosity was preserved after introduction of Co and Mo. This was observed for both N_2/H_2 and H_2/H_2S activated samples. In both cases, the shape of the hysteresis loop changes and corresponds to the formation of ink-bottle pores. This effect is characteristic of a percolation phenomenon caused by small Co/MoS₂ particles settling within the mesopores [39]. Moreover, a shift to smaller P/P_0 values for the onset of the hysteresis loop is observed indicating the presence of smaller pore diameters reflecting the filling of pores by sulfide particles. Table 2 reports the specific surface areas, pore volumes and pore diameter values of the SBA-15 support alone and of the different activated samples. Surface areas normalized per weight of silica and the normalized pore values are also reported in Table 2.

Table 2

Specific surface areas (SSA), pore volumes (V_p) and pore diameter (D) values of the SBA-15 support and of N_2/H_2 activated (set 1) and H_2/H_2S activated (set 2) SBA-15-supported CoMo catalysts. The values given into parentheses for the surface areas are the values per gram of support instead of per gram of catalyst.

Catalyst	SSA		V_p (cm^3/g)		D (Å)
	(m^2/g)	Normalized	(cm^3/g)	Normalized	
SBA-15	992	1.0	1.2	1.0	71
S1A	432 (573)	0.58	0.52	0.57	37
S1B	472 (624)	0.63	0.54	0.60	42
S1C	457 (604)	0.61	0.52	0.57	37
S2A	408 (540)	0.54	0.46	0.51	40
S2B	466 (616)	0.62	0.49	0.54	38
S2C	405 (536)	0.54	0.47	0.52	40

The surface area of the SBA-15 support reaches a very high value of $992 m^2/g$. After introduction of Co and Mo, the surface area decreases showing that porosity was partly blocked by the filling of the mesopores by Co/MoS₂ particles. However, specific surface areas remain high ranging between 400 and $470 m^2/g$. This effect can also be more clearly observed if considering surface areas per gram of support. In this case, values ranging between 540 and $624 m^2/g_{support}$ are obtained showing a decrease of about 40–45% of the surface area of the support due to pore filling. The decrease in surface area also seems slightly more important for H_2/H_2S activated samples leading to lower normalized values. This was confirmed when analyzing the evolution of pore volumes and pore diameters. While the SBA-15 support presents average pore diameter of about 7 nm, a shift to smaller pore diameters was observed for both H_2/N_2 or H_2/H_2S activated samples with similar values around 4 nm. This result confirms the location of Co/MoS₂ particles inside the mesopores of the SBA-15 support in both cases. Similarly, the use of the N_2/H_2 atmosphere leads to slightly higher pore volumes for a given temperature of treatment. Considering these data, it can be observed that by using the N_2/H_2 atmosphere during activation, similar or even slightly better textural properties of CoMo/SBA-15 catalysts could be obtained than using the traditional H_2/H_2S atmosphere.

3.1.2. X-ray diffraction

Fig. 2 shows the XRD patterns for set 1 (Fig. 2A) and for set 2 (Fig. 2B). All the XRD patterns present broad peaks corresponding to the poorly crystalline 2H-MoS₂ phase with signals at 2θ values of 14° , 33° , 40° and 58° corresponding to the (002), (100), (103) and (110) diffraction peaks. The amorphous silica leads to a broad peak at $2\theta = 22^\circ$. The different sets of catalysts exhibit relatively similar crystallinity whatever the atmosphere used during activation. Only a moderate increase in peak intensities can be observed with increasing temperature of treatment. However, this increase seems similar either after activation under H_2/H_2S or under N_2/H_2 . This point was confirmed through the determination of the stacking degree of MoS₂ slabs using the Scherrer equation applied to the (002) diffraction peak. Results are reported in Table 3. Stacking degree values vary in a narrow range between 4.6 and 5.1 for all the studied samples. A very moderate increase of the slab stacking with the temperature of treatment is observed whatever the mode of activation. However, this increase is more marked for N_2/H_2 activated samples leading to slightly higher stacking degrees after treatment at 773 and 823 K. It should also be noted that this

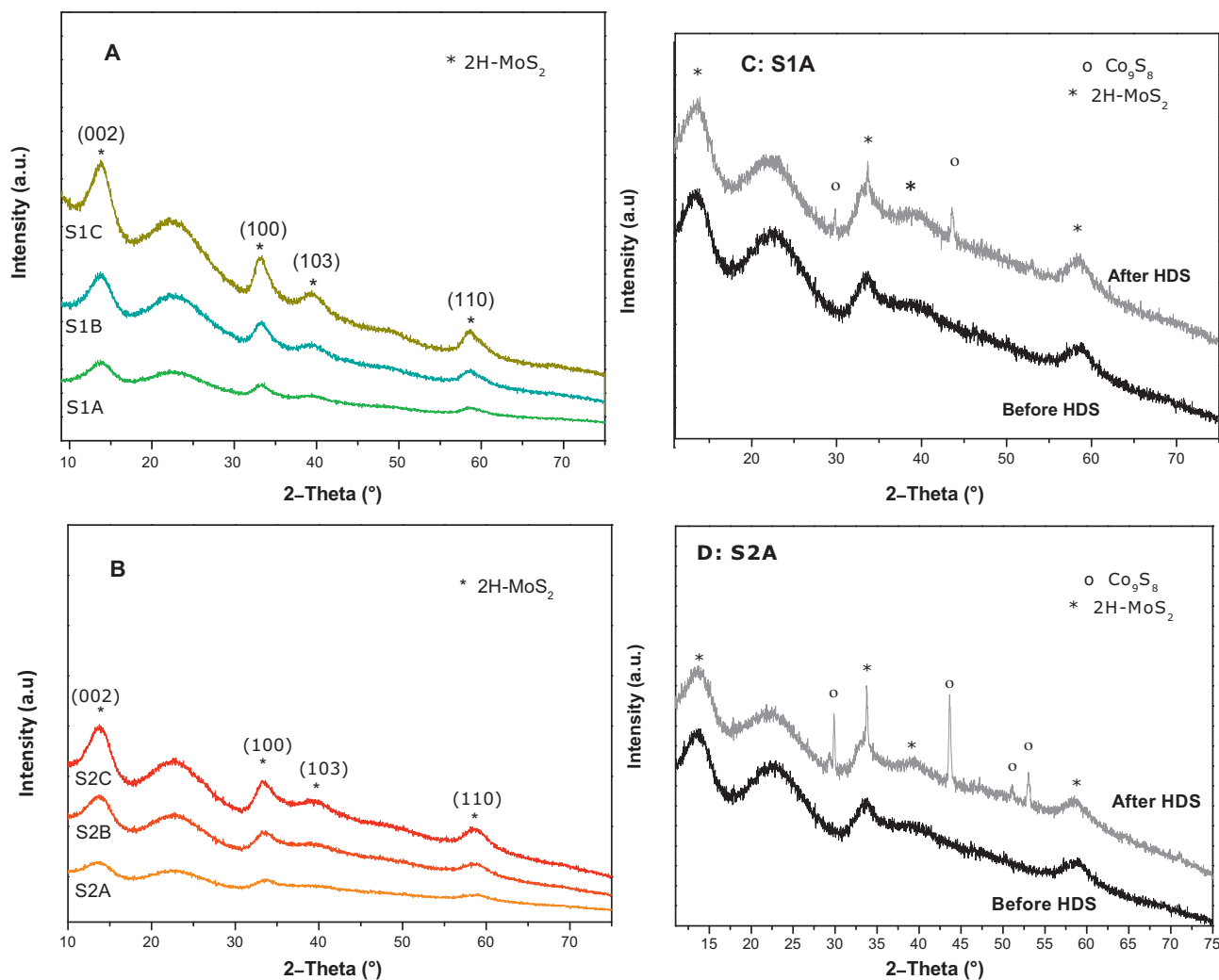


Fig. 2. XRD patterns (acquired before HDS) of the CoMo/SBA-15 samples obtained after activation under N_2/H_2 (set 1) (A) or under H_2/H_2S (set 2) (B). Comparison of the XRD patterns before and after HDS for the S1A sample activated under N_2/H_2 at 723 K (C) and for the S2A sample activated under H_2/H_2S at 723 K (D).

Table 3

Average stacking degrees of MoS_2 slabs (determined from XRD patterns) and slab length (determined by TEM) of the N_2/H_2 activated (set 1) and the H_2/H_2S activated (set 2) SBA-15-supported CoMo catalysts. The average stacking is determined by applying the Scherrer equation to the (002) MoS_2 diffraction peak and considering a value of 6.17 Å for the interlayer distance.

Catalyst	Average stacking degree (XRD)	Average slab length (nm, TEM)
S1A	4.6	5.2
S1B	4.9	10.3
S1C	5.1	20.1
S2A	4.7	9.5
S2B	4.7	10.0
S2C	4.9	7.3

increase in stacking remains weak taking into account the relatively high temperature of treatment used herein. This would be in agreement with a localization of the MoS_2 slabs inside the SBA-15 mesoporous material restraining their growth along the [001] direction. Finally, the absence of diffraction peaks due to cobalt sulfide suggests that the promoter atoms are well dispersed for the different sets of catalysts.

Fig. 2C and D shows respectively a comparison of the XRD patterns for CoMo/SBA-15 catalysts activated at the lowest temperature (723 K) using either the N_2/H_2 (S1A; Fig. 2C) or the H_2/H_2S atmosphere (S2A, Fig. 2D) before and after HDS reaction. In both

cases, diffraction peaks of the Co_9S_8 phase can be detected after HDS reaction. However, the crystallinity of the cobalt sulfide phase appears much more marked for the S2A sample activated under H_2/H_2S . This suggests that a higher proportion of cobalt was not initially in interaction with the edges of MoS_2 slabs leading after HDS to a higher tendency to sintering. Therefore, the activation under H_2/H_2S seems to lead to CoMo catalytic systems less stable under HDS reaction conditions.

3.1.3. Scanning electron microscopy

The morphology of the activated catalysts was also characterized by FE-SEM. The morphology of the CoMo/SBA-15 catalysts appears agglomerated (Fig. 3). Compared to the SBA-15 support alone, this could be in line with the decrease of surface area observed by N_2 physisorption measurements (Table 2). However, some differences can also be noticed when comparing the 723 K-activated S1A and S2A samples obtained respectively from a N_2/H_2 or a H_2/H_2S treatment. For the S1A sample (Fig. 3A), the characteristic well-ordered hexagonal arrays of honeycomb-like SBA-15 mesopores can be clearly observed. On the opposite, a denser morphology was found for the S2A sample (Fig. 3B) while the support porosity is not detected anymore. This result suggests that the N_2/H_2 treatment was less harmful for preserving an ordered porosity of the CoMo/SBA-15 catalysts than the H_2/H_2S activation.

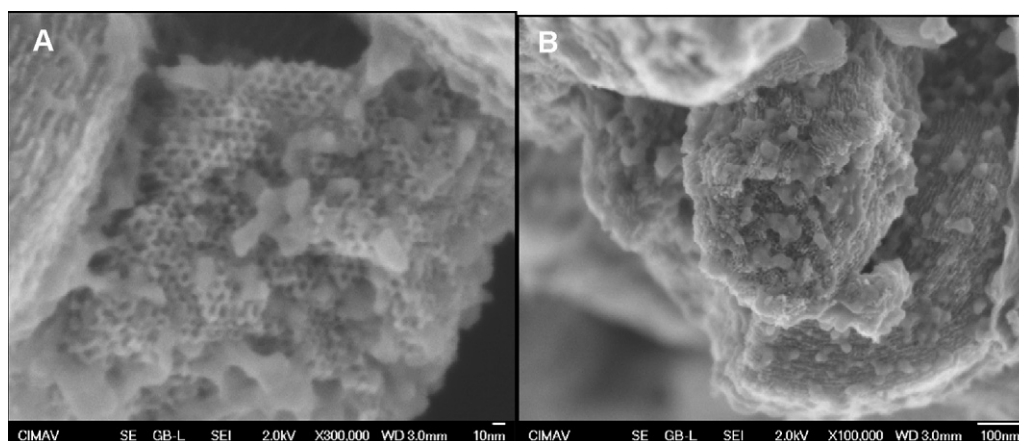


Fig. 3. Scanning electron micrographs of (A) the S1A sample activated under N_2/H_2 at 723 K and (B) the S2A sample activated under H_2/H_2S at 723 K.

3.1.4. Transmission electron microscopy

The CoMo/SBA-15 catalysts activated using either N_2/H_2 or H_2/H_2S atmosphere have also been characterized by transmission electron microscopy. Fig. 4a and b presents TEM pictures acquired respectively for the 723 K activated samples obtained under N_2/H_2 (S1A) or under H_2/H_2S (S2A). The SBA-15 channels with a diameter of about 5 nm can be clearly discerned on TEM pictures. The distance between two consecutive centers of hexagonal opening of channels, as estimated from TEM images, is close to the average pore size obtained by N_2 adsorption measurements. The MoS_2 slabs are in their vast majority located in a homogeneous way inside the channels of the SBA-15 support whatever the post-treatment atmosphere suggesting that the use of successive impregnations of the cobalt diethyldithiocarbamate precursor and of ATM are an efficient way to distribute the Co/ MoS_2 particles inside the SBA-15 mesoporosity. Only few slabs can be detected outside the SBA-15 channels (Fig. 4a).

This result is interesting since it shows the ability to obtain homogeneously cobalt-promoted MoS_2 nanoparticles inside the SBA-15 channels. Compared to previous studies [10,25], this shows the interest of using ATM solution to disperse homogeneously MoS_2 nanoparticles inside SBA-15 channels if an appropriate post-treatment is used contrary to the classical heptamolybdate impregnation approach [26]. This also represents an improvement compared to our previous study [10] for which cobalt acetate was used leading to an inhomogeneous dispersion inside this mesoporous material. Apparently, the use of an already-sulfided cobalt precursor is able to enhance the final dispersion of the active phase.

Statistics about the slab length were carried out for each CoMo/SBA-15 catalyst activated at 723 K, 773 K or 823 K using either a N_2/H_2 or H_2/H_2S atmosphere. It should be noted here that only slab length estimation was performed directly on TEM pictures and not the evaluation of the stacking degree. Indeed, in previous studies [6,40], synchrotron XRD (SR-XRD) techniques were found by some of us to be the most efficient method to determine the complete morphology (slab length, stacking degree) of supported MoS_2 nanoparticles. Moreover, comparison performed between SR-XRD results and estimation of particle size from TEM images led us to conclude that direct measurements on micrographs are a reliable approach for evaluating slab length along the basal direction. However, this comparison also emphasized a strong overestimation of the stacking degree when using only TEM statistics. This is related to the ability of TEM to detect about only 10% of the MoS_2 particles present on a support leading to a selective detection of the most stacked slabs [41].

Results show that after activation at 723 K, the Co/ MoS_2 nanoparticles obtained after treatment under N_2/H_2 present

Table 4

Activity, selectivity (HYD/DDS ratios), and turnover frequency values in the hydrodesulfurization of dibenzothiophene for the N_2/H_2 activated (set 1) and the H_2/H_2S activated (set 2) SBA-15-supported CoMo catalysts.

Catalyst	k (specific) ($1 \times 10^{-7} \text{ mol s}^{-1} \text{ g}^{-1}$)	HYD/DDS ratio	TOF (10^{-2} s^{-1})
S1A	19.2	0.25	2.6
S1B	16.8	0.25	4.2
S1C	15.0	0.23	7.1
S2A	12.3	0.18	2.8
S2B	13.9	0.21	3.4
S2C	16.4	0.23	3.0

smaller average slab length than those obtained under H_2/H_2S (5.2 nm vs 9.5 nm) (Table 3). After activation at 773 K, similar slab lengths are obtained whatever the atmosphere used to activate the CoMo/SBA-15 catalysts. While after activation under N_2/H_2 , the size doubled when increasing the temperature of treatment by 50 K for 723–773 K, the slab dimensions of H_2/H_2S activated samples remain relatively constant. Similar conclusions can be reached after activation at 823 K. While the slab length of the CoMo/SBA-15 catalyst activated under N_2/H_2 still doubled compared to the similar solid but activated at 773 K, the slab length of the H_2/H_2S activated samples even slightly decreased. However, it should be kept in mind that, except for the S1C sample (N_2/H_2 ; 823 K), the slab lengths measured in the present study appear smaller than those reported previously using ATM but with cobalt acetate [10]. A propensity to a better dispersion (particularly if activated under H_2/H_2S) is therefore observed if using the already sulfided cobalt diethyldithiocarbamate. When activated under N_2/H_2 , the sintering of the MoS_2 slabs then occurs only along the slab direction while preceding XRD results did not show any significant increase of the stacking degree. This 1D sintering process indirectly confirms the localization of the MoS_2 slabs inside the SBA-15 channels.

3.2. Catalytic activity in HDS reaction

Table 4 reports the DBT HDS activity of the different CoMo/SBA-15 catalysts obtained by activation under N_2/H_2 or H_2/H_2S at the different temperatures of treatment (723, 773, and 823 K). The N_2/H_2 activated catalysts exhibit higher activities than their H_2/H_2S activated counterparts at low temperatures of treatment (723 and 773 K). This is particularly the case for the S1A sample obtained by activation under N_2/H_2 at 723 K ($19.2 \times 10^{-7} \text{ mol s}^{-1} \text{ g}^{-1}$) with an activity 56% higher than for the same catalyst but activated under H_2/H_2S . Comparison to XRD results suggests that this higher activity is partly due to a higher stability of the cobalt-promoted

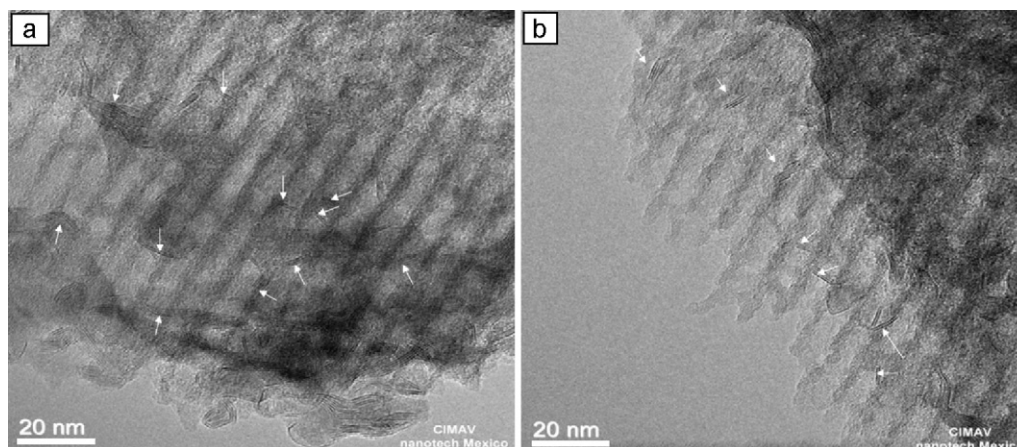


Fig. 4. Transmission electron micrographs of (A) the S1A sample activated under N_2/H_2 at 723 K and (B) the S2A sample activated under H_2/H_2S at 723 K.

phase under HDS conditions after the N_2/H_2 treatment leading to a smaller segregation effect. However, with the increase of the temperature of treatment, the activity tends to decrease moderately for the N_2/H_2 activated solids. On the opposite, a 30% increase in activity is observed for the H_2/H_2S activated catalysts when increasing the temperature from 723 K to 823 K. Therefore, after activation at 773 K, the N_2/H_2 activated solid is only 20% more active than the H_2/H_2S activated catalyst while after activation at 823 K, the H_2/H_2S activated CoMo/SBA-15 becomes more active.

With the increasing temperature of treatment, the decrease in activity of the N_2/H_2 activated CoMo/SBA-15 catalysts reflects the progressive formation of bigger MoS_2 slabs resulting in a lower proportion of Mo edge active sites. Similarly, the higher activity of the S2C sample activated at 823 K in comparison with the same H_2/H_2S activated catalysts but treated at lower temperatures mainly reflects a smaller average slab length and therefore a higher percentage of edge active sites. This point can be more clearly emphasized if calculating turnover frequency values taking into account the number of Mo edge active sites as determined from the MoS_2 hexagonal model developed by Kasztelan et al. [42]. In this case, relatively similar TOF values were obtained for the set of H_2/H_2S activated CoMo/SBA-15 catalysts. This would be in agreement with the fact that the increase in activity only results from a higher number of edge active sites and not to any improvement of the intrinsic activity per site, i.e. the quality of these sites. Interestingly, the determination of the TOF values for the N_2/H_2 activated catalysts shows an opposite evolution to the H_2/H_2S activation case. A strong increase in TOF values can be observed when increasing the temperature of treatment from 723 K to 773 K and finally to 823 K with values respectively of 2.6, 4.2, and $7.1 \times 10^{-2} s^{-1}$. Therefore, while active sites are not more intrinsically active for the N_2/H_2 activated catalyst after treatment at 723 K compared to the H_2/H_2S activation case, the use of an N_2/H_2 atmosphere at higher temperatures of treatment to activate our CoMo/SBA-15 catalysts can substantially improve the intrinsic activity per site allowing to partly compensate the lower percentage of edge active sites due to sintering of the active phase. These combined effects lead to a lower loss in activity than expected if considering only the increase of the MoS_2 particle size.

These results are also interesting if compared to our previous attempts to prepare CoMo/SBA-15 catalysts. In this respect, Nava et al. [26] tried initially to prepare CoMo/SBA-15 starting from ammonium heptamolybdate and cobalt nitrate. The DBT HDS activity obtained ($10.8 \times 10^{-7} mol s^{-1} g^{-1}$) (similar Co and Mo loadings) appears significantly lower than in the present case even if compared to the less active S2A catalyst. One possible reason was due

to the formation of Co/ MoS_2 particles outside the SBA-15 channels or to a poor dispersion of the active phase due to a restrained filling of the mesopores when using Mo oxide precursors and/or cobalt nitrate. The replacement of ammonium heptamolybdate by ATM led to the synthesis of CoMo/SBA-15 catalysts better dispersed into the SBA-15 channels but still inhomogeneously [10]. As a result, the activity of CoMo/SBA-15 catalysts (with 10 wt% Mo and 2 wt% Co) increases up to 13.1 and $13.7 \times 10^{-7} mol s^{-1} g^{-1}$ using SBA-15 with respectively pore diameters of 6 and 9 nm, therefore presenting activities similar to the H_2/H_2S activated S2A and S2B samples. Combination of two already sulfided Mo and Co precursors (ATM and cobalt diethyldithiocarbamate) in the present study led to a substantially higher HDS activity if an optimized N_2/H_2 activation procedure is used. This could be related to the better dispersion of the active phase inside SBA-15 channels using these sulfided precursors allowing to take benefit in a larger extent of the high surface mesoporous SBA-15 material.

The analysis of selectivity results expressed as HYD/DDS ratios shows relatively similar values whatever the samples ranging between 0.18 and 0.25 (Table 4). These results are in agreement with those obtained by Huang et al. [10] on CoMo/SBA-15 catalysts obtained by using ATM and cobalt acetate but differ from those acquired by Nava et al. [26] on similar CoMo/SBA-15 catalysts but prepared using ammonium heptamolybdate and cobalt nitrate (HYD/DDS=0.40). Therefore, in the present case, the as-obtained CoMo/SBA-15 catalysts exhibit a depleted HYD activity. These results could be first analyzed taking into account the Rim-Edge model [43]. According to this model, the DBT HDS selectivity along the DDS route leading to biphenyl or along the HYD route leading to cyclohexylbenzene is controlled by the stacking degree of the MoS_2 nanoparticles, the more the nanoparticles are stacked, the less the resulting catalyst will be hydrogenating. The reason for such a selectivity variation would be related to the accessibility of edge sites to the DBT molecule. The pre-requisite for the hydrogenation of the phenyl ring of the DBT molecule would be a sterically demanding η^6 flat adsorption mode possible only on external layers of MoS_2 particles (called rim sites) while the steric hindrance of internal layers would lead to an absence of hydrogenation on these sites (called edge sites). On the opposite, the pre-requisite for the C–S bond rupture step would be the $\eta^1(S)$ adsorption mode possible on both rim and edge sites.

In the present case, the similar HYD/DDS ratios obtained whatever the samples would be in agreement with the absence of significant variation of the stacking degree. However, a deeper analysis of these results can also be made. Indeed, whatever the sample considered, a depleted HYD selectivity is obtained which appeared

particularly marked if compared to results previously acquired on industrial CoMo/Al₂O₃ catalysts (0.49) [26]. As already observed by Huang et al. [10] and Nava et al. [26], this depleted HYD character is in fact related to a confinement effect of Co/MoS₂ nanoparticles inside the mesoporosity of the SBA-15 support. Indeed, the localization of the particles inside the mesopores hinders the possibility for the DBT molecule to adsorb in a sterically demanding η⁶ flat adsorption and therefore to be hydrogenated leading to an enhancement of the DDS selectivity. This effect observed for SBA-15 supported catalysts was also observed systematically for MoS₂ [44,45], Co/MoS₂ [36,46] and Ni/MoS₂ [47] nanoparticles loaded in carbon mesopores. The development of a carbon mesoporous organization led to depleted HYD selectivity whatever the MoS₂-based catalysts to be formed.

In this respect, it is interesting to observe that similar HYD/DDS ratios were obtained by Huang et al. [10] for which cobalt-promoted MoS₂ nanoparticles were mainly located inside the SBA-15 channels even if inhomogeneously dispersed. Similarly, the presence of Co-promoted MoS₂ nanoparticles outside the SBA-15 channels [26] could explain the higher hydrogenating character observed for CoMo/SBA-15 catalysts prepared using Mo oxide precursors and cobalt nitrate.

4. Conclusions

The synthesis of CoMo/SBA-15 catalysts was herein performed using a novel approach using already-sulfided Mo and Co precursors, ammonium tetrathiomolybdate and cobalt diethyldithiocarbamate allowing to homogeneously disperse a high proportion of cobalt-promoted MoS₂ nanoparticles inside SBA-15 channels. Optimization of the activation parameters (temperature of treatment, atmosphere) was subsequently carried out in order to enhance catalytic properties. Compared to the classical H₂/H₂S atmosphere, the use of a N₂/H₂ atmosphere allows to obtain better stabilized Co/MoS₂ nanoparticles for which cobalt segregation under hydrodesulfurization conditions is limited. Moreover, depending on the atmosphere used, the temperature of activation differently influences the morphology of the active phase leading to a rapid monodimensional sintering at high temperature under N₂/H₂ while its influence is hardly noticed under H₂/H₂S. The combination of using already sulfided Co and Mo precursors with the optimization of the activation procedure led to highly active CoMo/SBA-15 catalysts. Finally, the localization of cobalt-promoted MoS₂ nanoparticles inside the mesopores of the SBA-15 support led to confinement effects and to more direct desulfurization selective catalytic systems.

Acknowledgments

The authors acknowledge CONACyT for financial support (Project 26067), and PAPIIT project IN102509-3, the National Nanotechnology Laboratory (NANOTECH), Chihuahua, México and Red de Nanociencias y Nanotecnología, the valuable technical assistance from W. Antunez, C. Ornelas, and E. Torres and E. Aparicio.

References

[1] CE bulletin n° 715/2007 of the European parliament and council, 20/06/07.

- [2] H. Topsøe, B.S. Clausen, F.E. Massoth, in: J.R. Anderson, M. Boudart (Eds.), *Hydrotreating Catalysis and Science and Technology*, vol. 11, Springer-Verlag, Berlin/Heidelberg, 1996.
- [3] C.N. Satterfield, *Heterogeneous Catalysis in Industrial Practice: Catalyst Preparation and Manufacture*, second edition, Krieger Publishing Co., 1996, pp.87–129.
- [4] H. Shimada, *Catal. Today* 86 (2003) 17–29.
- [5] Y. Sakashita, Y. Araki, H. Shimada, *Appl. Catal. A: Gen.* 215 (2001) 101–110.
- [6] G. Berhault, M. Perez De la Rosa, A. Mehta, M. José-Yacamán, R.R. Chianelli, *Appl. Catal. A: Gen.* 345 (2008) 80–88.
- [7] M. Breyse, G. Berhault, S. Kasztelan, M. Lacroix, F. Mauge, G. Pérot, *Catal. Today* 66 (2001) 15–22.
- [8] Y.V. Joshi, P. Ghosh, M. Daage, W.N. Delgass, *J. Catal.* 257 (2008) 71–80.
- [9] I. Eswaramoorthi, V. Sundaramurthy, N. Das, A.K. Dalai, J. Adjaye, *Appl. Catal. A: Gen.* 339 (2008) 187–195.
- [10] Z.-D. Huang, W. Bensch, L. Kienle, S. Fuentes, G. Alonso, C. Ornelas, *Catal. Lett.* 122 (2008) 57–67.
- [11] Y. Saih, K. Segawa, *Appl. Catal. A: Gen.* 353 (2009) 258–265.
- [12] M. Breyse, P. Afanasiev, C. Geantet, M. Vrinat, *Catal. Today* 86 (2003) 5–16.
- [13] T. Chiranjeevi, P. Kumar, S.K. Maity, M.S. Rana, G. Murali Dhar, T.S.R. Prasad Rao, *Microporous Mesoporous Mater.* 44 (2001) 547–556.
- [14] G. Pérot, *Catal. Today* 86 (2003) 111–128.
- [15] R. Prada Silvy, F. Delannay, P. Grange, B. Delmon, *Polyhedron* 5 (1986) 195–198.
- [16] M. Wojciechowska, M. Pietrowski, B. Czajka, S. Łomnicki, *Catal. Lett.* 87 (2003) 153–157.
- [17] R.D. Mičić, R.P. Marinković-Nedučín, Z. Schay, I. Nagy, M. Hadnadev, E.E. Kiss, *Rev. Roum. Chim.* 53 (2008) 629–634.
- [18] Z.D. Huang, W. Bensch, A. Lotnyk, L. Kienle, S. Fuentes, J. Bocarando, G. Alonso, C. Ornelas, *J. Mol. Catal. A: Chem.* 323 (2010) 45–51.
- [19] S. Texier, G. Berhault, G. Pérot, V. Harlé, F. Diehl, *J. Catal.* 223 (2004) 404–418.
- [20] S. Texier, G. Berhault, G. Pérot, F. Diehl, *Appl. Catal. A: Gen.* 293 (2005) 105–119.
- [21] J. Van Gestel, J. Légli, J.C. Duchet, *J. Catal.* 145 (1994) 429–436.
- [22] Y. Okamoto, K. Hioka, K. Arakawa, T. Fujikawa, T. Ebihara, T. Kubota, *J. Catal.* 268 (2009) 49–59.
- [23] H. Farag, A.N.A. El-Hendawy, K. Sakanishi, M. Kishida, I. Mochida, *Appl. Catal. B: Environ.* 91 (2009) 189–197.
- [24] B. Pawelec, R. Navarro, J.L.G. Fierro, P.T. Vasudevan, *Appl. Catal. A: Gen.* 168 (1998) 205–217.
- [25] E.J.M. Hensen, P.J. Kooyman, Y. Van der Meer, A.M. van der Kraan, V.H.J. de Beer, J.A.R. van Veen, R.A. van Santen, *J. Catal.* 199 (2001) 224–235.
- [26] R. Nava, R.A. Ortega, G. Alonso, C. Ornelas, B. Pawelec, J.L.G. Fierro, *Catal. Today* 127 (2007) 70–84.
- [27] D. Valencia, T. Klimova, *Catal. Today* 166 (2011) 91–101.
- [28] L. Vradman, M.V. Landau, M. Herskowitz, V. Ezersky, M. Talianker, S. Nikitenko, Y. Koltypin, A. Gedanken, *J. Catal.* 213 (2003) 163–175.
- [29] K. Ramanathan, S.W. Weller, *J. Catal.* 95 (1985) 249–259.
- [30] P.T. Vasudevan, S.W. Weller, *J. Catal.* 99 (1986) 235–238.
- [31] S. Fuentes, G. Diaz, F. Pedraza, H. Rojas, N. Rosas, *J. Catal.* 113 (1988) 535–539.
- [32] J. Cruz-Reyes, M. Avalos-Borja, M.H. Farias, S. Fuentes, *J. Catal.* 137 (1992) 232–242.
- [33] P.T. Vasudevan, F. Zhang, *Appl. Catal. A: Gen.* 112 (1994) 161–173.
- [34] K. Wilkinson, M.D. Merchán, P.T. Vasudevan, *J. Catal.* 171 (1997) 325–328.
- [35] Y. Yoneyama, C. Song, *Catal. Today* 50 (1999) 19–27.
- [36] H. Nava, C. Ornelas, A. Aguilar, G. Berhault, S. Fuentes, G. Alonso, *Catal. Lett.* 86 (2003) 257–265.
- [37] R. Huirache-Acuña, M.A. Albitzer, C. Ornelas, F. Paraguay-Delgado, R. Martínez-Sánchez, G. Alonso-Núñez, *Appl. Catal. A: Gen.* 308 (2006) 134–142.
- [38] F.J. Brieler, P. Grundmann, M. Fröba, L.M. Chen, P.J. Klar, W. Heimbrot, H.A.K. von Nidda, T. Kurz, A. Loidl, *J. Am. Chem. Soc.* 126 (2004) 797–807.
- [39] N. Mizuno, M. Misono, *Chem. Rev.* 98 (1998) 199–218.
- [40] M. Perez De la Rosa, S. Texier, G. Berhault, A. Camacho, M.J. Yacamán, A. Mehta, S. Fuentes, J.A. Montoya, F. Murrieta, R.R. Chianelli, *J. Catal.* 225 (2004) 288–299.
- [41] R.R. Chianelli, A.F. Ruppert, M.J. Yacamán, A. Vazquez-Zavala, *Catal. Today* 23 (1995) 269–281.
- [42] S. Kasztelan, A. Wambeke, L. Jalowiecki, J. Grimblot, J.P. Bonnelle, *J. Catal.* 124 (1990) 12–21.
- [43] M. Daage, R.R. Chianelli, *J. Catal.* 149 (1994) 414–427.
- [44] G. Alonso, G. Berhault, A. Aguilar, V. Collins, C. Ornelas, S. Fuentes, R.R. Chianelli, *J. Catal.* 208 (2002) 359–369.
- [45] G. Alonso, M.H. Siadati, G. Berhault, A. Aguilar, R.R. Chianelli, *Appl. Catal. A: Gen.* 263 (2004) 109–117.
- [46] L. Alvarez, J. Espino, C. Ornelas, J.L. Rico, M.T. Cortez, G. Berhault, G. Alonso, *J. Mol. Catal. A: Chem.* 210 (2004) 105–117.
- [47] L. Alvarez, G. Berhault, G. Alonso, *Catal. Lett.* 125 (2008) 35–45.